
Exploring Inductive Biases in Contrastive Learning: A Clustering Perspective

Yunzhe Zhang

Zhejiang University of Technology
xsgx1z@live.cn

Yao Lu

Zhejiang University of Technology
yaolu.zjut@gmail.com

Lei Xu

Zhejiang University of Technology
aaaaalei@outlook.com

Kunlin Yang

Zhejiang University of Technology
ykl.zjut@gmail.com

Hui Tang

Zhejiang University of Technology
huitang.zjut@gmail.com

Shuyuan Ye

Zhejiang University of Technology
ysyx077@163.com

Qi Xuan

Zhejiang University of Technology
xuanqi@zjut.edu.cn

Abstract

This paper investigates the differences in data organization between contrastive and supervised learning methods, focusing on the concept of locally dense clusters. We introduce a novel metric, Relative Local Density (RLD), to quantitatively measure local density within clusters. Visual examples are provided to highlight the distinctions between locally dense clusters and globally dense ones. By comparing the clusters formed by contrastive and supervised learning, we reveal that contrastive learning generates locally dense clusters without global density, while supervised learning creates clusters with both local and global density. We further explore the use of a Graph Convolutional Network (GCN) classifier as an alternative to linear classifiers for handling locally dense clusters. Finally, we utilize t-SNE visualizations to substantiate the differences between the features generated by contrastive and supervised learning methods. We conclude by proposing future research directions, including the development of efficient classifiers tailored to contrastive learning and the creation of innovative augmentation algorithms. Our code is available at this site.

1 Introduction

Contrastive learning has significantly influenced machine learning by learning representations from unlabeled data, thereby edging us closer to the goal of building models that can generalize across diverse data distributions and tasks. However, a comprehensive conceptual understanding of this phenomenon is yet to be established. Recent research efforts ([2], [41], [17], [44]) have aimed to bridge this gap by analyzing properties of augmented views and their distributions, making assumptions, and providing mathematical proofs to justify the contrastive loss function.

However, these assumptions, often based on intuition, may not align with real-world data distributions. For instance, [36] highlights that in practice, there is often little overlap between the distributions of

augmented views, regardless of class membership, making assumptions like those in [44] potentially incorrect.

We address this by examining the role of inductive bias in contrastive loss from a clustering perspective. We note that contrastive learning forms cluster distinct from those generated by supervised learning due to its inductive bias. Our key observations are:

- In contrastive learning, visually similar images have similar vector representations, even if they belong to different classes. Conversely, visually dissimilar images from the same class have distinct representations.
- This leads to the formation of locally dense clusters for images from the same class, while visually different images of the same class are not globally clustered. We propose a metric called "RLD (Relative Local Density)" to quantify this property.
- The local density of clusters poses a challenge for linear classifiers. Hence, we propose using a GCN classifier, which performs better for most models due to the locally dense clustering nature of contrastive learning.

2 Related Work and Preliminaries

2.1 Understanding Contrastive Learning

Contrastive learning, which learns representations from similar data pairs, has shown impressive results in downstream tasks. These pairs are generated using temporal information ([43], [28]) or different augmentations of inputs ([21], [15], [18], [13], [7], [45], [40], [6], [3]). By minimizing a contrastive loss, the similarity of a representation across various 'views' of the same image is maximized, while minimizing similarity with distracting negative samples.

Multiple views can be obtained naturally from multimodal data ([1], [24], [30], [32], [33], [39]), or through cropping and data augmentation for image-only modalities ([3], [20], [21], [31], [6], [11], [13], [18], [45]). Positive pairs are views of the same data point, and negatives are sampled views of different data points, although the need for negative samples has been debated ([7], [16], [46]).

Many studies have explored contrastive learning, with early works assuming that positive samples are (nearly) conditionally independent and establishing a bound on contrastive loss and classification performance ([37], [26]). Later work [44] posited an overlap between intra-class augmented views and provided a bound for downstream performance.

However, [36] argued that neglecting inductive biases leads to an inadequate understanding of contrastive learning's success and can even result in vacuous guarantees. This work also highlighted the minimal overlap between the distributions of augmented images, contradicting assumptions in previous works.

Armed with this understanding, we will examine the role of inductive biases and their effect on clustering and classification performance.

2.2 Cluster and Community Evaluation

In this paper, clusters are defined as distinct subsets within a data partition, each representing a group of similar data points. Cluster evaluation, a long-standing question ([22], [38]), often focuses on cluster structure [35] or consistency with ground truth labels [34]. We primarily address the former, considering true labels as a partition.

Traditionally, well-structured clusters are expected to be "dense and well-separated". The Calinski-Harabasz score or Variance Ratio Criterion [5] quantifies this:

$$\text{CH score} = \frac{\sum_{i=1}^k n_i \|\mu_i - \mu\|^2 / (k - 1)}{\sum_{i=1}^k \sum_{x \in C_i} \|x - \mu_i\|^2 / (n - k)} \quad (1)$$

where k is the cluster count, n the data point count, n_i the count in cluster C_i , μ_i the centroid of C_i , and μ the overall centroid. The score is the ratio of between-cluster to within-cluster dispersion, with

dispersion defined as the sum of squared distances. However, as we’ll show, this score doesn’t suit clusters formed by contrastive learning, prompting an alternative cluster concept.

Here, communities serve as cluster analogs in graphs rather than Euclidean space. Modularity [8] is a common community quality metric, quantifying internal connections density versus expected random connections density. For graph G with adjacency matrix $A \in \mathbb{R}^{N \times N}$, modularity Q is:

$$Q = \frac{1}{2m} \sum_{i,j} \left[A_{ij} - \frac{k_i k_j}{2m} \right] \delta(y_i, y_j) \quad (2)$$

where m is the sum of edge weights, k_i and k_j are nodes i and j degrees, y_i and y_j are nodes i and j community assignments, and $\delta(y_i, y_j)$ is the Kronecker delta function. Our experiments suggest that with appropriate G construction, modularity can better reveal contrastive learning cluster structures.

2.3 Graph Convolutional Network

Graph Convolutional Networks (GCNs) are neural networks specifically designed for graph-structured data, gaining traction due to their proficiency in learning from this data type ([23], [4], [9]). This paper focuses on the GCN architecture proposed by [23], which underpins many other GCN models and encapsulates key characteristics of GCN models.

Graph-structured data typically includes node features $X \in \mathbb{R}^{N \times C}$ and an adjacency matrix $A \in \mathbb{R}^{N \times N}$, where N is the number of nodes and C is the node feature dimensions. A GCN maps the input node features X to new node features $Z \in \mathbb{R}^{N \times F}$, where F is the output feature dimension. The GCN proposed by [23] performs graph convolutions as follows:

$$Z = \sigma \left(\tilde{A} X W \right), \quad (3)$$

where $\tilde{A} = \hat{D}^{-\frac{1}{2}} \hat{A} \hat{D}^{-\frac{1}{2}}$, with $\hat{A} = A + I_N$ and \hat{D} is the diagonal degree matrix of \hat{A} . $W \in \mathbb{R}^{C \times F}$ is a learnable weight matrix, and $\sigma(\cdot)$ is an element-wise activation function.

For a deeper GCN with L layers, the output feature matrix $Z^{(L)}$ is computed through a series of graph convolutions:

$$Z^{(l)} = \sigma \left(\tilde{A} Z^{(l-1)} W^{(l)} \right), \quad (4)$$

where $l = 1, \dots, L$, $Z^{(0)} = X$, and $W^{(l)} \in \mathbb{R}^{F_{l-1} \times F_l}$ are learnable weight matrices for each layer. The dimensions of the input and output features change through layers, with $F_0 = C$ and $F_L = F$.

We modify the GCN by introducing a learnable scale parameter α in each layer, transforming the adjacency matrix as $\hat{A} = \alpha A + I_N$. This allows for dynamic balancing between self-connections and connections to neighboring nodes, potentially enhancing the network’s ability to extract valuable information from the graph structure. The updated adjacency matrix \tilde{A} becomes:

$$\tilde{A} = \hat{D}^{-\frac{1}{2}} (\alpha A + I_N) \hat{D}^{-\frac{1}{2}}, \quad (5)$$

This modified \tilde{A} enables the GCN to better adjust to the underlying graph structure during training, as it learns the optimal value of α alongside the weight matrices W .

Due to its compatibility with graph space, we utilize a GCN as the classifier. This makes it a better fit for the characteristics of clusters formed by contrastive learning. Our experiments show that the GCN surpasses a linear classifier in various scenarios, further affirming its suitability in this context.

3 Experimental Settings

This section presents our experimental setup for training models on the CIFAR-10 dataset [25]. We base our framework on [1] and enhance it with [14]’s prediction head, using a 512-dimension

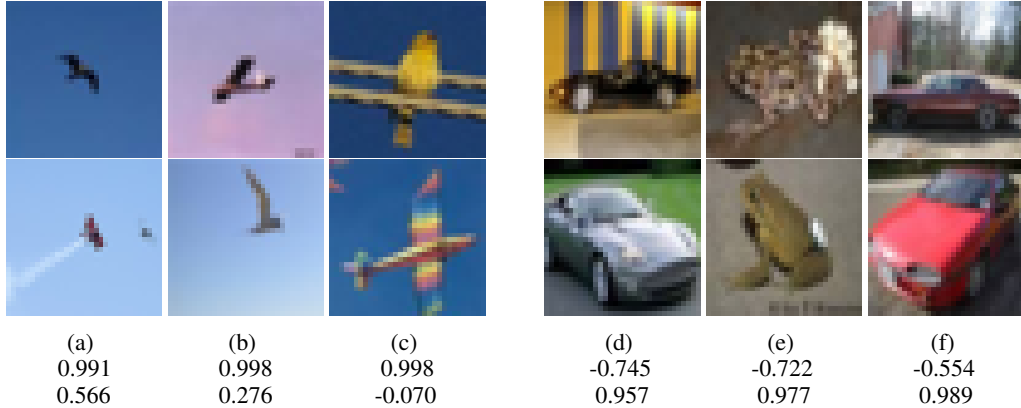


Figure 1: **Exploring Image Pairs and Their Cosine Similarities in Representations.** (a) displays the image pair with the highest similarity across different labels in contrastive ResNet18, while (b) demonstrates the same for ResNet101, and (c) for ViT. In contrast, (d) illustrates the image pair with the lowest similarity within the same class in contrastive ResNet18, (e) for ResNet101, and (f) for ViT. The first line beneath each image pair indicates the similarity in contrastive space, and the second line denotes the similarity in supervised space (using a supervised model with the same architecture). In (a), the top image portrays a bird, and the bottom one depicts an airplane. The blue sky backgrounds and dark main bodies contribute to their visual similarity. Contrastive ResNet18 has difficulty distinguishing them, whereas supervised ResNet18 can. This observation also applies to (b) and (c). Conversely, (d), (e), and (f) present pairs of visually distinct images (including hue, shape, perspective, etc.) within the same class, which are recognized by supervised models but not by contrastive models.

representation space. The tested model architectures include ResNet18, ResNet101, and a modified Vision Transformer comparable to ResNet101 in parameter count ([19], [12]). For benchmarking, we train three models with identical architectures using CIFAR-10 supervised learning, also with a 512-dimension representation. All models use the AdamW optimizer [29]. Detailed architecture and hyperparameter information is in the appendix. Experiments run on a single A100 GPU.

In the following sections, we extract image vector representations from raw dataset images using both contrastive and supervised models, per standard evaluation practices. All features are normalized to unit vectors due to the undefined lengths during the training process.

We note that our experimental setup is not fine-tuned for peak performance. Consequently, our focus is not on achieving record-breaking results. Instead, we aim to gain new insights into contrastive learning’s inner mechanisms, rather than proposing practical enhancements or techniques.

4 Micro View: Image Pairs Under Contrastive Learning

This section explores how contrastive and supervised learning methods organize images within the representation space. Our analysis investigates how these methods group images based on visual similarities and class labels. We first highlight contrastive learning’s ability to group visually similar images, regardless of their class labels, then discuss the class label focused organization of images in supervised learning, which may overlook visual similarities within and across classes. We also examine the properties of k-nearest neighbors in the contrastive representation space and introduce the Class Homogeneity Index (CHI) to quantify the average proportion of k-nearest neighbors with the same class label. By comparing CHI across different models under both learning methods, we offer insights into both local and global class homogeneity of neighborhoods in the representation space, and how architectural choices affect contrastive learning behavior.

4.1 Contrastive Representation Space and Visual Similarity

We scrutinize specific image pairs from the CIFAR-10 training dataset to demonstrate the distinct properties of contrastive representation space. Figures 1a, 1b, and 1c depict image pairs from different

Table 1: **CHI across diverse models under contrastive and supervised learning.** The table presents the Class Homogeneity Index (CHI) for diverse models—ResNet18, ResNet101, and ViT—under both contrastive and supervised learning conditions, across different k values.

CHI	Contrastive			Supervised		
	ResNet18	ResNet101	ViT	ResNet18	ResNet101	ViT
k=1	0.8938	0.8818	0.8730	0.9680	0.9611	0.9903
k=10	0.8762	0.8662	0.8473	0.9674	0.9611	0.9893
k=100	0.8457	0.8438	0.8047	0.9669	0.9605	0.9886
k=500	0.7785	0.7945	0.6675	0.9666	0.9605	0.9881
k=1000	0.7094	0.7267	0.5273	0.9663	0.9606	0.9879

classes with the highest cosine similarity in contrastive space, while Figures 1d, 1e, and 1f present image pairs from the same class with the lowest similarity.

Obviously, in contrastive space, image pairs showcasing visual resemblance exhibit high similarity, irrespective of their class. Conversely, pairs with similar class labels but disparate visual appearances have a low similarity. This trend is not mirrored in supervised space, where class labels primarily dictate similarity, rather than visual attributes.

We attribute this discrepancy to the unsupervised nature of contrastive learning, which leans on inherent sample information, while supervised learning relies heavily on provided labels to establish image relationships.

4.2 Minimal Overlap Between Visually Similar Images

Previously we observed that contrastive learning effectively groups visually similar images. This raises a question: Is the grouping a result of overlapping distributions of augmented views for these images? [44] posits that visually similar images have overlapping augmented view distributions and that’s why they are grouped.

Formally, let x_1 and x_2 be visually similar images, and $f(y|x)$ be the probability density function of the augmented distribution for a given image x . It’s suggested that there’s at least one \hat{y} for which $f(\hat{y}|x_1)f(\hat{y}|x_2) > 0$, indicating distribution overlap, driving the similarity of x_1 and x_2 in contrastive representations.

Here, we aim to quantify this overlap. We use $P(y_1 = y_2 | y_1 \sim f(y|x_1), y_2 \sim f(y|x_2))$ as our metric, representing the probability that two augmented views, y_1 and y_2 , are equal, drawn from x_1 and x_2 ’s distributions. Higher values indicate more overlap.

The Monte Carlo method is employed to approximate this probability for image pairs from Figures 1a, 1b, and 1c, generating 100,000,000 pairs of augmented views for each. Our analysis reveals no overlap—no identical augment pairs. With the Clopper-Pearson method, we calculate a 95% confidence interval for the proportion, yielding an upper bound of 3.69×10^{-8} .

This result indicates minimal overlap in the augmented views of visually similar images. Hence, the ability of contrastive learning to group visually similar images may stem from inductive biases like the model’s ability to capture similar high-level features, not direct overlap in augmented data.

4.3 K-Nearest Neighbors in Contrastive Representation Space

As we’ve seen in the previous subsections, contrastive learning tends to group visually similar images together, regardless of their class labels. However, empirically, it is reasonable to assume that for most images, their visually similar counterparts belong to the same class. So we can then infer that most representations have neighbors with the same label in contrastive space.

Delving into the properties of the k-nearest neighbors for each data point within the contrastive representation space, we use cosine similarity as our distance metric and compute the average proportion of k-nearest neighbors that share the same class, a metric we term the Class Homogeneity Index (CHI). We explore the effects of varying k values ($k = 1, 10, 100, 500, 1000$) on CHI and summarize our findings in Table 1.

Several implications emerge from Table 1. First, for smaller k values, the high CHI observed in contrastive learning underscores that nearest neighbors typically belong to the same class. This significant feature further validates the proposition: in the contrastive representation space, most representations have neighbors with the same label.

Second, the steep decrease in CHI as k increases in contrastive learning compared to supervised learning reveals an intriguing attribute. The neighborhood’s class-wise homogeneity in the contrastive representation space seems to diminish more rapidly as we expand our neighborhood size. This implies that while contrastive features exhibit a local class-wise homogeneity, they do not extend this effect at a more global scale, unlike the supervised features.

Third, the most noticeable decline in CHI is observed for the ViT. This could indicate that its weaker inductive bias is a contributing factor. Therefore, the behavior of contrastive learning might be shaped not only by the data but also by architectural choices and their inherent inductive biases.

5 Macro View: Contrastive Learning Forms Locally Dense Clusters

Moving on from the individual image analysis, we now focus on how contrastive learning arranges data at a larger scale, at the cluster level. We introduce a new concept of "Locally Dense" clusters, where data points within the same class are closely packed. As a result, a specific data point’s nearest neighbors are predominantly from its own cluster, leading to high class homogeneity within local regions of the cluster. We propose a new graph-based metric, the Relative Local Density (RLD), to quantify this local density.

Next, we illustrate what locally dense clusters look like and how they differ from "dense and well-separated" clusters. The latter refers to clusters that are not just densely packed internally but are also clearly separated from other clusters, implying a global density and separation.

Finally, we show that contrastive learning forms clusters that are locally dense but not globally, while supervised learning clusters exhibit both local and global density and separation.

5.1 Relative Local Density: A Quantitative Measure for Locally Dense Clusters

While the qualitative notion of locally dense clusters provides a conceptual foundation, it leaves room for a concrete, quantifiable measure. Thus, we introduce RLD, a novel metric aimed at capturing the notion of local density. This subsection details the construction of RLD, illuminating its correspondence to local density and its unique advantages.

The computation of RLD involves several stages, each contributing to the encapsulation of local density. Initially, we construct a similarity matrix, S , for a given set of data points X . Each entry, S_{ij} , captures the pairwise distance between data points X_i and X_j , normalized by the mean distance and the square root of the dimension of X to ensure scale-invariance:

$$S_{ij} = \frac{-dist(X_i, X_j)}{\sqrt{dim(X)} \cdot mean(dist(X_p, X_q) : p, q \in 1, 2, \dots, n, p \neq q)} \quad (6)$$

This process converts distances into similarity scores, with higher scores indicating closer data points. The matrix diagonal elements are set to negative infinity, ensuring a data point does not regard itself as its neighbor.

The similarity matrix is then transformed into an adjacency matrix, A , which encapsulates the relationships between data points in the feature space. A temperature parameter, T , modulates this transformation, balancing the emphasis on local and global structures. A higher T yields a matrix with a more global structure, while a lower T retains more local information. The matrix is normalized, each entry divided by T and exponentially transformed to accentuate differences between data points:

$$A_{ij} = \frac{n^2 \cdot exp(S_{ij}/T)^2}{\sum_{k=1}^n exp(S_{ik}/T)^2 \cdot \sum_{k=1}^n exp(S_{kj}/T)^2} \quad (7)$$

The final RLD computation step measures the modularity of the adjacency matrix concerning class labels, y , with equation 2. Modularity, a graph theory concept purposed by [8], quantifies the strength

of a graph’s division into clusters. A high modularity score signifies dense intra-cluster connections and sparse inter-cluster connections, aligning with our local density intuition.

The RLD thus quantifies local density, gauging a cluster’s internal cohesion relative to its separation. As a cluster evaluation metric, RLD offers several advantages:

1. **Local structure emphasis:** Unlike global metrics like the CH score, RLD captures local structure details, offering a more fine-grained data organization understanding.
2. **Differentiability:** RLD’s full differentiability enables integration into optimization processes, including gradient-based learning.
3. **Scale invariance:** RLD’s insensitivity to the scale and number of data points enhances its versatility across diverse datasets.
4. **Graph techniques compatibility:** RLD’s graph-based nature permits integration with other graph techniques, such as community detection and graph partitioning. This expands the analysis range and can yield additional cluster structure insights.
5. **Comparability:** The modularity scaling to $(-0.5, 1)$ standardizes RLD, facilitating comparisons. Its application enables direct cluster comparison, as scores are relative to the same scale.

5.2 Visualizing Locally Dense Clusters: Examples and Comparisons

To gain a more intuitive understanding of local and global density concepts, it’s important to visualize them before delving into the cluster analysis formed by contrastive and supervised learning methods. To facilitate this, we introduce illustrative examples that distinguish between locally dense clusters, as determined by RLD, and globally dense ones, as gauged by the CH score.

Figure 2 presents six distinct cluster examples, each illustrating the divergent nature of local and global densities. Let’s examine some key observations:

1. A high RLD doesn’t guarantee a high CH score. This fact is exemplified by clusters (b), (c), and (d), which, despite their high RLDs, register significantly lower CH scores compared to clusters (e) and (f).
2. The CH score fails to acknowledge the well-structured nature of clusters (b) and (c). This observation underscores the insensitivity of the CH score to certain types of cluster formations.
3. Clusters (b), (c), and (d) pose challenges for linear classifiers, which often struggle to define linear boundaries effectively. On the other hand, these classifiers are likely to perform well with clusters (e) and (f). Conversely, classifiers that operate in a neighbor-centric space, such as KNN, may deliver better separation results for clusters (b), (c), and (d).

5.3 Comparing Clusters Formed by Contrastive Learning and Supervised Learning

With a solid understanding of local and global density concepts, we can now turn our attention to examining the clusters produced by contrastive and supervised learning methods.

To provide a comprehensive and dynamic picture of cluster formation, we consider not only clusters created by fully trained models but also those formed during the training process which enables us to capture the evolution of clusters throughout the training phase and observe the unique ways in which different learning methods shape them over time.

In Figure 3 (a) and (b), we present a synthesized analysis. The RLDs ($T = 0.1$) and CH scores for all contrastive and supervised features are displayed in relation to linear classifier accuracy, along with their respective Spearman correlation coefficients. This collective view provides a comparative perspective on how these learning methods impact data organization.

As demonstrated in Figure 3 (a), there is a visible positive correlation between the CH score of supervised learning and linear classifier accuracy. In contrast, contrastive learning shows a negative correlation and maintains a nearly constant CH score throughout the entire training process. This observation suggests that contrastive learning does not create globally dense clusters.

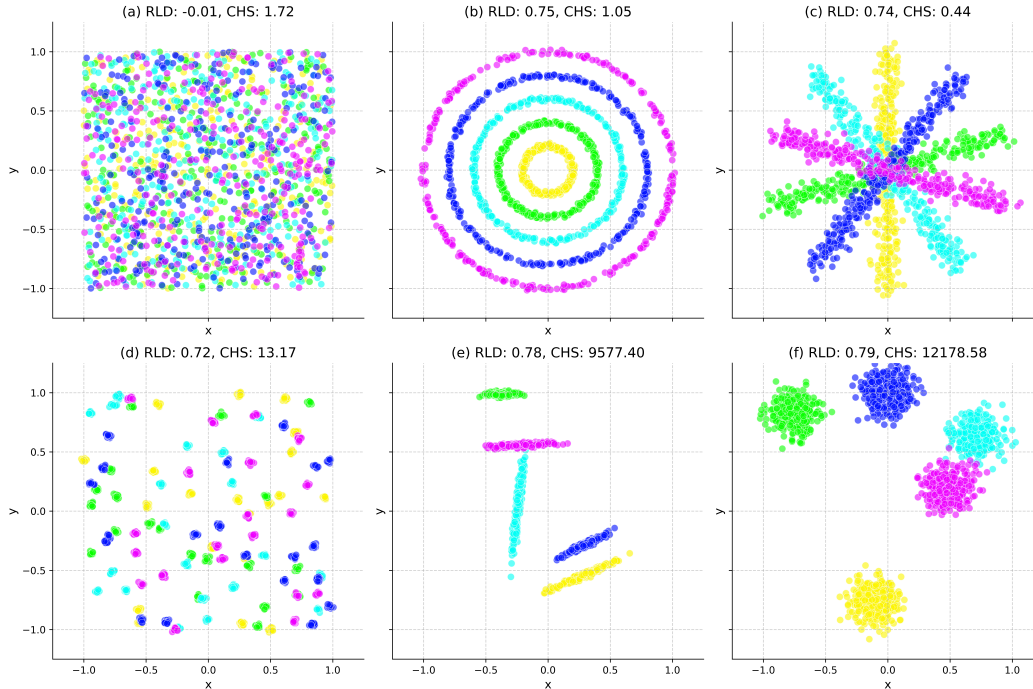


Figure 2: **Varied Cluster Configurations and Their Corresponding RLDs and CH scores.** Each subfigure, from (a) to (f), symbolizes a unique cluster configuration. Subfigure (a) presents data points uniformly scattered without discernible clustering, whereas (b) demonstrates a circular pattern with identifiable local clusters. Subfigure (c) showcases clusters arranged along distinct lines, and (d) displays small, tightly grouped local clusters dispersed throughout the plot. Subfigure (e) illustrates clusters formed along random lines, while (f) portrays multiple Gaussian distributions, each constituting a separate cluster. These examples underscore the varied characteristics of local and global densities and highlight the limitations of relying solely on global metrics, like the CH score, for evaluating cluster quality.

However, as depicted in Figure 3 (b), the Spearman correlation between linear classifier accuracy and RLD remains positive for both learning methods, even almost the same given the same architecture. This result implies that both contrastive learning and supervised learning form locally dense clusters.

Applying a GCN Classifier Given the challenges faced by linear classifiers in distinguishing locally dense clusters, as observed in Figure 2 (b), (c), and (d), we decided to explore the use of a GCN classifier as an alternative. To facilitate this, we first constructed a graph identical to the one used in the computation of the RLDs. When assigning node features, we utilized a one-hot encoding scheme. Each node was assigned a one-hot encoded vector of length equal to the number of classes. In this scheme, each vector represented a specific class label, with the element corresponding to the class label set to 1, and all other elements set to 0.

Following the training method described in [23], we applied a random mask rate sampled from (0.05, 0.5) and use a three-layer GCN. The model accuracy is then plotted in Figure 3 (c), comparing it with linear accuracy. The results indicate that for the ResNet101 and ViT, GCN accuracy is slightly higher than linear accuracy for most of the models, although the opposite is observed for the ResNet18. This suggests that a GCN classifier can sometimes outperform linear classifiers in contrastive learning.

Visual Evidence via t-SNE Lastly, we employ t-SNE [42] as a visualization tool to further illustrate the differences between the features generated by contrastive and supervised learning methods. t-SNE is known for its ability to manage both 'local' and 'global' views via a tunable parameter known as perplexity. When we adjust this parameter in Figure 4, it becomes evident that contrastive clusters start to fade as the perplexity increases. This effect, however, is not observed in the clusters formed

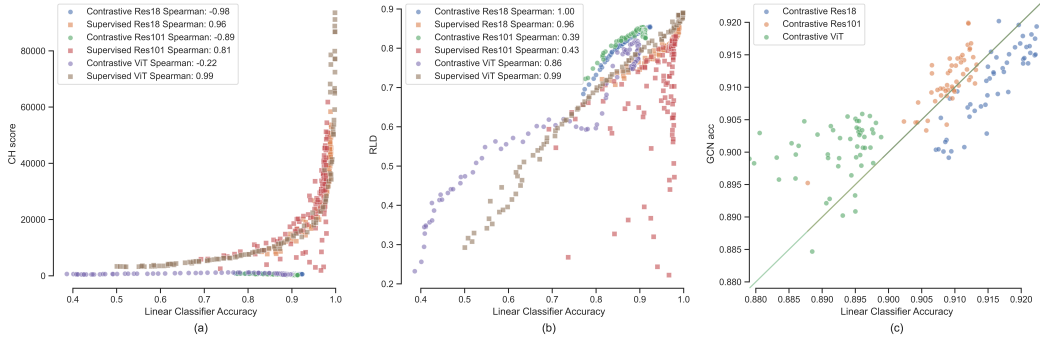


Figure 3: Comparative Analysis of Cluster Evaluation Metrics and Classifier Accuracy across Models. The figure presents three scatter plots comparing different metrics with linear classifier accuracy for contrastive and supervised learning methods across three models: ResNet18, ResNet101, and ViT. (a) shows the correlation between CH scores and linear classifier accuracy. (b) illustrates the relationship between RLD and linear classifier accuracy. (c) provides a comparison between GCN classifier accuracy and linear classifier accuracy for contrastive learning models.

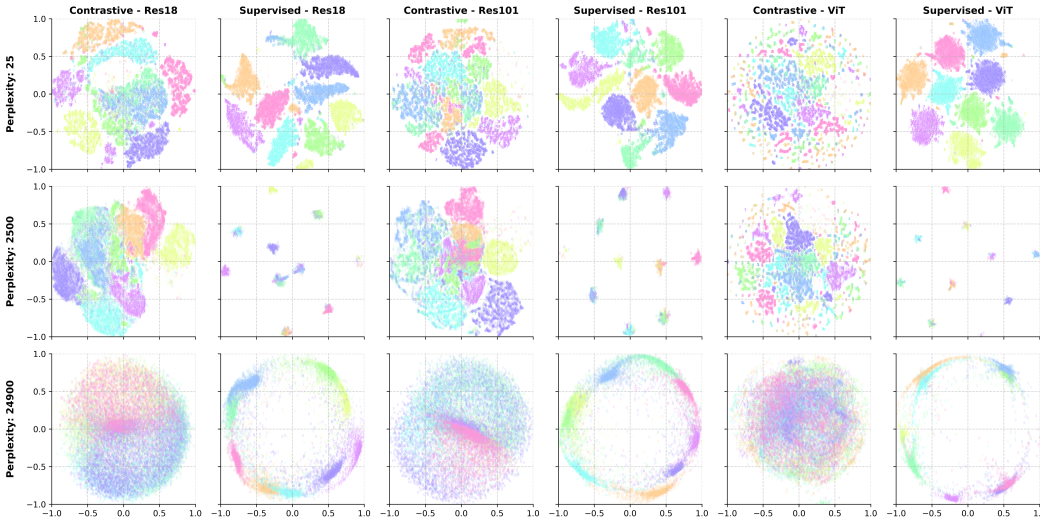


Figure 4: t-SNE Visualization of Features Generated by Contrastive and Supervised Learning. This figure presents t-SNE visualizations of 25,000 data points for contrastive (left column) and supervised (right column) learning methods, across three different model architectures: ResNet18, ResNet101, and ViT. Each row corresponds to a different perplexity value (25, 2500, and 24900), showcasing the influence of this parameter on the visualization.

by supervised learning, thereby reinforcing our earlier observations about the distinct differences between these two types of learning methods.

6 Conclusion and Future Directions

This study illuminates distinct differences in how contrastive and supervised learning algorithms structure data in representational space. We discover that contrastive learning primarily fosters 'locally dense' clusters, irrespective of class labels, while supervised learning tends to generate globally dense clusters that align with class labels. The novel RLD metric introduced in this study quantifies local density, offering a contrast to the traditional Calinski-Harabasz score. Implementing a GCN classifier demonstrates potential in tackling locally dense clusters, and the differences between learning methods are further highlighted through t-SNE visualizations.

Looking ahead, we propose two potential research directions. First, the development of more efficient classifiers tailored to clusters created by contrastive learning should be a priority. While GCNs show promise, their computational and memory requirements present challenges. Second, creating innovative augmentation algorithms could help prevent models from misclassifying visually similar images from different classes by distinguishing these images in augmented views.

7 Limitations

While our study provides insightful findings, it is not without its constraints. Resource limitations prevented us from evaluating a wider array of model architectures, such as the Swin Transformer [27], or utilizing larger datasets like ImageNet [10]. Further exploration of these areas is suggested for future research endeavors.

References

- [1] R. Arandjelovic and A. Zisserman. Look, listen and learn. In *Proceedings of the IEEE international conference on computer vision*, pages 609–617, 2017.
- [2] S. Arora, H. Khandeparkar, M. Khodak, O. Plevrakis, and N. Saunshi. A theoretical analysis of contrastive unsupervised representation learning. In *36th International Conference on Machine Learning, ICML 2019*, pages 9904–9923. International Machine Learning Society (IMLS), 2019.
- [3] P. Bachman, R. D. Hjelm, and W. Buchwalter. Learning representations by maximizing mutual information across views. *Advances in neural information processing systems*, 32, 2019.
- [4] J. Bruna, W. Zaremba, A. Szlam, and Y. LeCun. Spectral networks and deep locally connected networks on graphs. In *2nd International Conference on Learning Representations, ICLR 2014*, 2014.
- [5] T. Caliński and J. Harabasz. A dendrite method for cluster analysis. *Communications in Statistics-theory and Methods*, 3(1):1–27, 1974.
- [6] T. Chen, S. Kornblith, M. Norouzi, and G. Hinton. A simple framework for contrastive learning of visual representations. In *International conference on machine learning*, pages 1597–1607. PMLR, 2020.
- [7] X. Chen and K. He. Exploring simple siamese representation learning. In *Proceedings of the IEEE/CVF conference on computer vision and pattern recognition*, pages 15750–15758, 2021.
- [8] A. Clauset, M. E. Newman, and C. Moore. Finding community structure in very large networks. *Physical review E*, 70(6):066111, 2004.
- [9] M. Defferrard, X. Bresson, and P. Vandergheynst. Convolutional neural networks on graphs with fast localized spectral filtering. In *Proceedings of the 30th International Conference on Neural Information Processing Systems*, pages 3844–3852, 2016.
- [10] J. Deng, W. Dong, R. Socher, L.-J. Li, K. Li, and L. Fei-Fei. Imagenet: A large-scale hierarchical image database. In *2009 IEEE conference on computer vision and pattern recognition*, pages 248–255. Ieee, 2009.
- [11] C. Doersch and A. Zisserman. Multi-task self-supervised visual learning. In *Proceedings of the IEEE international conference on computer vision*, pages 2051–2060, 2017.
- [12] A. Dosovitskiy, L. Beyer, A. Kolesnikov, D. Weissenborn, X. Zhai, T. Unterthiner, M. Dehghani, M. Minderer, G. Heigold, S. Gelly, et al. An image is worth 16x16 words: Transformers for image recognition at scale. In *International Conference on Learning Representations*, 2020.
- [13] A. Dosovitskiy, J. T. Springenberg, M. Riedmiller, and T. Brox. Discriminative unsupervised feature learning with convolutional neural networks. *Advances in neural information processing systems*, 27, 2014.

- [14] Y. Dubois, S. Ermon, T. B. Hashimoto, and P. S. Liang. Improving self-supervised learning by characterizing idealized representations. *Advances in Neural Information Processing Systems*, 35:11279–11296, 2022.
- [15] T. Gao, X. Yao, and D. Chen. Simcse: Simple contrastive learning of sentence embeddings. In *Proceedings of the 2021 Conference on Empirical Methods in Natural Language Processing*, pages 6894–6910, 2021.
- [16] J.-B. Grill, F. Strub, F. Altché, C. Tallec, P. Richemond, E. Buchatskaya, C. Doersch, B. Avila Pires, Z. Guo, M. Gheshlaghi Azar, et al. Bootstrap your own latent—a new approach to self-supervised learning. *Advances in neural information processing systems*, 33:21271–21284, 2020.
- [17] J. Z. HaoChen, C. Wei, A. Gaidon, and T. Ma. Provable guarantees for self-supervised deep learning with spectral contrastive loss. *Advances in Neural Information Processing Systems*, 34:5000–5011, 2021.
- [18] K. He, H. Fan, Y. Wu, S. Xie, and R. Girshick. Momentum contrast for unsupervised visual representation learning. In *Proceedings of the IEEE/CVF conference on computer vision and pattern recognition*, pages 9729–9738, 2020.
- [19] K. He, X. Zhang, S. Ren, and J. Sun. Deep residual learning for image recognition. In *Proceedings of the IEEE conference on computer vision and pattern recognition*, pages 770–778, 2016.
- [20] O. Henaff. Data-efficient image recognition with contrastive predictive coding. In *International conference on machine learning*, pages 4182–4192. PMLR, 2020.
- [21] R. D. Hjelm, A. Fedorov, S. Lavoie-Marchildon, K. Grewal, P. Bachman, A. Trischler, and Y. Bengio. Learning deep representations by mutual information estimation and maximization. In *International Conference on Learning Representations*, 2018.
- [22] L. Hubert and P. Arabie. Comparing partitions. *Journal of classification*, 2:193–218, 1985.
- [23] T. N. Kipf and M. Welling. Semi-supervised classification with graph convolutional networks. In *International Conference on Learning Representations*, 2016.
- [24] B. Korbar, D. Tran, and L. Torresani. Cooperative learning of audio and video models from self-supervised synchronization. *Advances in Neural Information Processing Systems*, 31, 2018.
- [25] A. Krizhevsky and G. Hinton. Learning multiple layers of features from tiny images. Technical Report 0, University of Toronto, Toronto, Ontario, 2009.
- [26] J. D. Lee, Q. Lei, N. Saunshi, and J. Zhuo. Predicting what you already know helps: Provable self-supervised learning. *Advances in Neural Information Processing Systems*, 34:309–323, 2021.
- [27] Z. Liu, Y. Lin, Y. Cao, H. Hu, Y. Wei, Z. Zhang, S. Lin, and B. Guo. Swin transformer: Hierarchical vision transformer using shifted windows. In *Proceedings of the IEEE/CVF international conference on computer vision*, pages 10012–10022, 2021.
- [28] L. Logeswaran and H. Lee. An efficient framework for learning sentence representations. In *International Conference on Learning Representations*, 2018.
- [29] I. Loshchilov and F. Hutter. Decoupled weight decay regularization. In *International Conference on Learning Representations*, 2017.
- [30] A. Miech, D. Zhukov, J.-B. Alayrac, M. Tapaswi, I. Laptev, and J. Sivic. Howto100m: Learning a text-video embedding by watching hundred million narrated video clips. In *Proceedings of the IEEE/CVF International Conference on Computer Vision*, pages 2630–2640, 2019.
- [31] A. v. d. Oord, Y. Li, and O. Vinyals. Representation learning with contrastive predictive coding. *arXiv preprint arXiv:1807.03748*, 2018.

- [32] A. Owens and A. A. Efros. Audio-visual scene analysis with self-supervised multisensory features. In *Proceedings of the European Conference on Computer Vision (ECCV)*, pages 631–648, 2018.
- [33] A. Recasens, P. Luc, J.-B. Alayrac, L. Wang, F. Strub, C. Tallec, M. Malinowski, V. Pătrăucean, F. Altché, M. Valko, et al. Broaden your views for self-supervised video learning. In *Proceedings of the IEEE/CVF International Conference on Computer Vision*, pages 1255–1265, 2021.
- [34] A. Rosenberg and J. Hirschberg. V-measure: A conditional entropy-based external cluster evaluation measure. In *Proceedings of the 2007 joint conference on empirical methods in natural language processing and computational natural language learning (EMNLP-CoNLL)*, pages 410–420, 2007.
- [35] P. J. Rousseeuw. Silhouettes: a graphical aid to the interpretation and validation of cluster analysis. *Journal of computational and applied mathematics*, 20:53–65, 1987.
- [36] N. Saunshi, J. Ash, S. Goel, D. Misra, C. Zhang, S. Arora, S. Kakade, and A. Krishnamurthy. Understanding contrastive learning requires incorporating inductive biases. In *International Conference on Machine Learning*, pages 19250–19286. PMLR, 2022.
- [37] N. Saunshi, O. Plevrakis, S. Arora, M. Khodak, and H. Khandeparkar. A theoretical analysis of contrastive unsupervised representation learning. In *International Conference on Machine Learning*, pages 5628–5637. PMLR, 2019.
- [38] A. Strehl and J. Ghosh. Cluster ensembles—a knowledge reuse framework for combining multiple partitions. *Journal of machine learning research*, 3(Dec):583–617, 2002.
- [39] C. Sun, A. Myers, C. Vondrick, K. Murphy, and C. Schmid. Videobert: A joint model for video and language representation learning. In *Proceedings of the IEEE/CVF international conference on computer vision*, pages 7464–7473, 2019.
- [40] Y. Tian, D. Krishnan, and P. Isola. Contrastive multiview coding. In *Computer Vision—ECCV 2020: 16th European Conference, Glasgow, UK, August 23–28, 2020, Proceedings, Part XI 16*, pages 776–794. Springer, 2020.
- [41] C. Tosh, A. Krishnamurthy, and D. Hsu. Contrastive learning, multi-view redundancy, and linear models. In *32nd International Conference on Algorithmic Learning Theory*, 2021.
- [42] L. van der Maaten and G. Hinton. Visualizing data using t-sne. *Journal of Machine Learning Research*, 9(86):2579–2605, 2008.
- [43] X. Wang and A. Gupta. Unsupervised learning of visual representations using videos. In *Proceedings of the IEEE international conference on computer vision*, pages 2794–2802, 2015.
- [44] Y. Wang, Q. Zhang, Y. Wang, J. Yang, and Z. Lin. Chaos is a ladder: A new theoretical understanding of contrastive learning via augmentation overlap. In *International Conference on Learning Representations*, 2022.
- [45] Z. Wu, Y. Xiong, S. X. Yu, and D. Lin. Unsupervised feature learning via non-parametric instance discrimination. In *Proceedings of the IEEE conference on computer vision and pattern recognition*, pages 3733–3742, 2018.
- [46] J. Zbontar, L. Jing, I. Misra, Y. LeCun, and S. Deny. Barlow twins: Self-supervised learning via redundancy reduction. In *International Conference on Machine Learning*, pages 12310–12320. PMLR, 2021.